Zeolites

DOI: 10.1002/anie.201105450

Atomic Resolution Analysis of Silver Ion-Exchanged Zeolite A**

Alvaro Mayoral, Thomas Carey, Paul A. Anderson, Axel Lubk, and Isabel Diaz*

Zeolites are crystalline microporous aluminosilicates based on AlO_4 and SiO_4 tetrahedra that are connected by shared oxygen atom bridges. Combinations of these tetrahedral structures lead to at least 176 unique zeolite framework types,[1] making zeolites the most important and versatile heterogeneous catalysts.[2] In reactions zeolites can select between reactants and products because of their pore shape, size, and distribution which determine their properties.[3] As a result zeolites are widely employed in the fields of petroleum refining and petrochemistry, and also as desiccants, ion exchangers, and molecular sieves, for example in water/air treatments.[4] In addition to their structure-related properties, they can also be employed as bifunctional catalysts when different metals are incorporated within the framework. To characterize these guest elements, conventional high-resolution transmission electron microscopy has been applied.[5] However, recording several micrographs from the same crystal has resulted in an almost impossible task, as most zeolites are tremendously sensitive to the electron beam. This sensitivity has been related to radiolytic damage,[5a,6] which decreases with increasing acceleration voltage.[5b] The most important factor limiting the lifetime of zeolites under electron beam irradiation is the Si/Al ratio. A Si-rich zeolite is more stable than one with a low Si/Al ratio. Furthermore, the type of cation incorporated into the framework has been found to have an influence on the sensitivity of the zeolite beam.[7]

In the case of scanning transmission electron microscopy (STEM) imaging, the scenario may be worse because the beam is concentrated on a very fine spot which can burn a hole above some threshold current density.[8] However, if a slightly different approach is made by using low-dose conditions, novel and excellent visual information can be achieved, especially in combination with aberration-corrected electron microscopes,[9] which can be used for dynamic imaging of single atoms[10] and clusters composed of a few atoms.[11]

The motivation for the present work rests on the application of spherical aberration-corrected high-angle annular dark-field STEM (C_s-corrected HAADF-STEM), where the contrast is related to Z^2 (atomic number) to study zeolite A (LTA structure type) which has an Si/Al ratio of 1:1 (the highest aluminum content possible and therefore the least stable zeolite under electron beam irradition). The incorporation of silver into this structure results in the formation of a material with antibacterial activity[12] and with particular applications for the recovery of radioactive materials.[13]

Here the Na^+ cations incorporated during the synthesis were replaced by Ag^+ ions,[14] followed by complete dehydration of the zeolites which results in a spectacular sequence of color changes from white, in its hydrated form, to orange when fully dehydrated.[15] Kim and Seff attributed this color change to the presence of partially reduced Ag_6 octahedra in the sodalite cages (Figure 1). In contrast, Jacobs et al.[16] proposed that the coloration was due to the presence of linear Ag_3 clusters (see top right cage in Figure 1). Figure 1 shows the proposed model for the dehydrated AgA (silver zeolite A) where the red atoms correspond to oxygen and the grey Ag atoms form an octahedron inside the sodalite cage

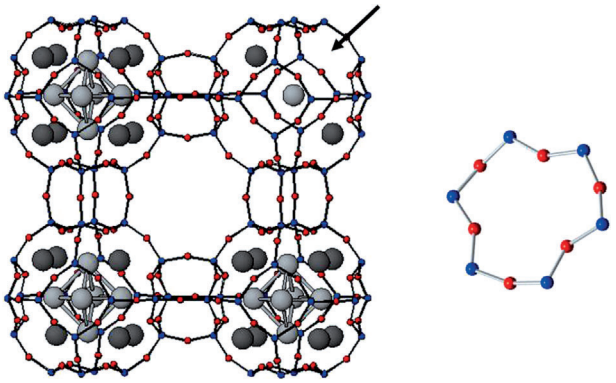

Figure 1. Ag_6 clusters in zeolite A (LTA), red atoms correspond to O and blue atoms correspond to Si and Al, coordinated by up to eight silver atoms. A linear Ag_3 unit is also shown in the cage on the top right. b) The 6-ring marked in (a) with a black arrow.

[*] Dr. A. Mayoral
Laboratorio de Microscopías Avanzadas (LMA)
Instituto de Nanociencia de Aragón (INA)
Universidad de Zaragoza, Mariano Esquillor
50018, Zaragoza (Spain)
E-mail: amayoral@unizar.es

T. Carey, Dr. P. A. Anderson
School of Chemistry, University of Birmingham
Edgbaston, Birmingham (UK)

Dr. A. Mayoral, Dr. A. Lubk
Transpyrenean Associated Laboratory for
Electron Microscopy (TALEM)

Dr. A. Lubk
CEMES-CNRS, Groupe NanoMatériaux, Toulouse (France)

I. Diaz
Instituto de Catálisis y Petroleoquímica, CSIC, Madrid (Spain)

[**] T.C. acknowledges the University of Birmingham, the EPRSC, and the Diamond Light Source for funding and the AWM/EDRF-funded Birmingham Science City Advanced Materials 1 project for providing facilities and equipment. Many thanks to the Diamond Light Source for the provision of powder synchrotron X-ray diffraction facilities and to Chiu Tang, Julia Parker, and Stephen Thompson for assistance in using beamline I11.

Supporting information for this article is available on the WWW under http://dx.doi.org/10.1002/anie.201105450.

with six to eight surrounding Ag atoms placed in the six rings (Figure 1b).

Here the crystallographic positions of zeolite groups and silver atoms were determined by Rietveld refinement against high-resolution XRD data (see the Supporting Information S1). When the materials, initially kept under inert atmosphere, were prepared for electron microscopy studies, they were in contact with air for a few minutes (during crushing and microgrid deposition).

For comparison both NaA (sodium zeolite A) and AgA (silver zeolite A) were imaged. Figure 2a shows the model for as-synthesized zeolite $A^{[1]} \mid Na^{+}_{12}(H_2O)_{27} \mid_8 [Al_{12}Si_{12}O_{48}]_8$ (for clarity only Si, Al, and O are shown). In this model, viewed along the [001] orientation, the red atoms, that is, the zeolite bridges, correspond to oxygen atoms. Due to the low stability of the zeolites under electron beam irradiation, the minimum exposure time was used for the images (8 seconds per image), using a beam current of 1.65×10^{-10} A. The larger alpha cages together with the smaller sodalite cages (center) are directly observed, and they are confirmed by comparison with the model shown and superimposed on the recorded image (Figure 2b) and on the simulated image (Figure 2c).

Figure 3 shows C_s-corrected STEM-HAADF images of dehydrated AgA along its main crystallographic orientations, [001], [011], and [111]. Due to the low stability of the zeolites under electron beam irradiation each orientation was recorded on different crystallites as severe beam damage occurred. For a typical scanning experiment, the zeolite damage always started on the edge of the particle, the thinnest area, and produced a loss of crystallinity (see the Supporting Information S2). Large differences were observed between this sample and the as-synthesized material. In the dehydrated AgA a perfect distribution of white spots coupled with the zeolite structure was observed. This extraordinary distribution was observed in all the crystallographic orientations (see Figure 3 and the Supporting Information S3) but no extra spots appeared in the fast Fourier transform (FFT) diffractogram. In addition, spheres with higher contrast, marked by white arrows in Figure 3b, were also observed in coincidence with the zeolite cages.

Further analysis of the NaA images in Figure 2 shows that the black parts correspond to the parts with no mass, that is, zeolite alpha cages, linked to each other by sodalite cages, in which the four-membered rings can clearly be observed. To interpret the raw data obtained by scanning transmission electron microscopy, we must assume that at this level, we cannot distinguish between the framework atoms as they are very similar in terms of atomic number. By superimposing the zeolite model the electron micrographs can easily be understood. The fact that the atoms forming the sodalite cage are

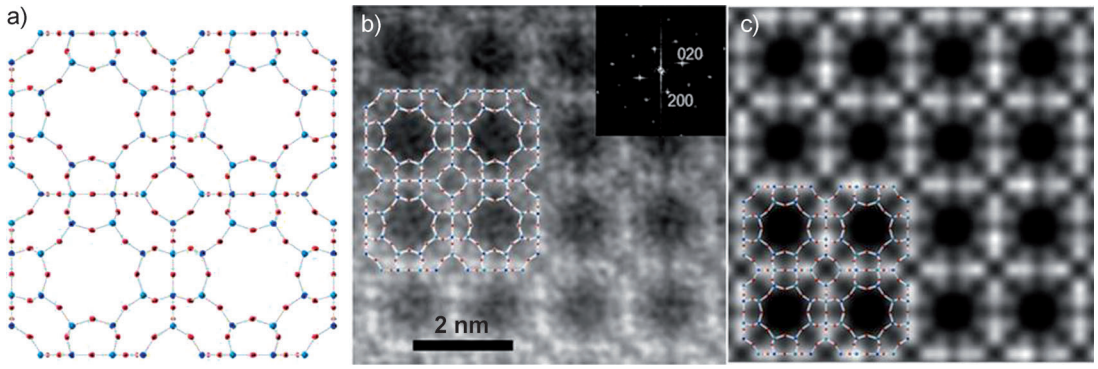

Figure 2. a) Model for the LTA framework, $Fm\bar{3}c$. b) Inverse FFT image recorded along the [001] direction. The FFT diffractogram, shown in the inset, was indexed assuming the $Fm\bar{3}c$ symmetry. c) Simulated HAADF-STEM image of the crystal framework along the [001] direction using multislice calculations. Parameters used: 300 kV, $C_s = 0$ mm, a defocus value of 0, a probe convergence angle of 24.5 mrad, and a collection angle of 50–200 mrad. The zeolite A unit cell is superimposed in parts (b) and (c).

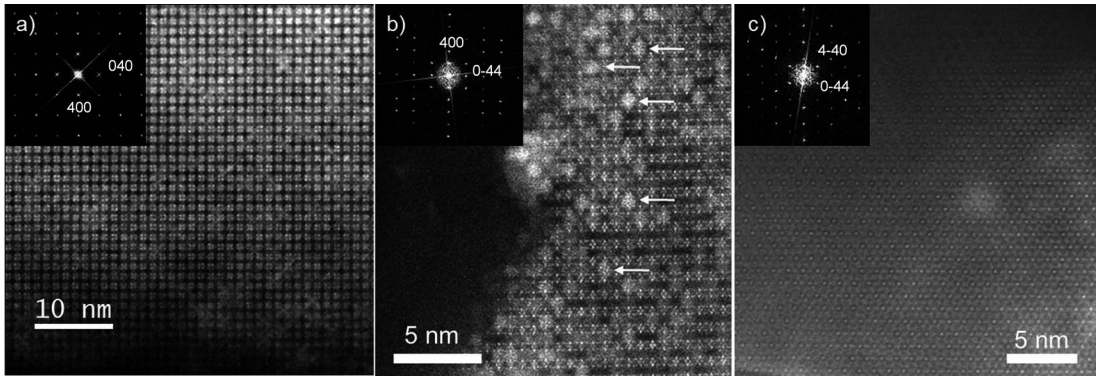

Figure 3. Aberration-corrected STEM-HAADF micrographs of dehydrated AgA recorded along a) [001], b) [011], and c) [111] directions.

faint and not completely resolved is a consequence of first, quick beam damage to the zeolite, which did not allow us to go to a higher resolution, and second, beam spread, which damaged the probe when the beam passed through the crystal. To get a well-fitted correlation between simulation and experiment the simulated HAADF image was convoluted with a Gaussian filter of 1.7 Å full width at half maximum (fwhm) in a last step, which effectively reduced the spatial resolution (see the Supporting Information S4).

The zeolitic framework of the ion-exchanged material (Figure 4) is virtually invisible because of the great difference in the atomic number of silver and the zeolitic framework, and only four atomic columns forming squares or nine columns[15a] were identified (Figure 4b). Figure 4b shows the atomic distribution where each unit contains nine Ag atomic columns. By measuring the distances between the atoms placed in the corners we obtained a value of around 4.72 Å, which can be attributed to Ag located at the 6-rings forming the sodalite cage. In the model obtained by Rietveld refinement, this distance was determined to be 4.76 Å (Figure 4c). Meanwhile, the distance between Ag columns in the adjacent sodalite cages was found to be approximately 7.41 Å, compared to 7.57 Å in the model. In addition to those four columns of atoms another, less bright, five atoms can be observed. These atoms which are situated one in the center of the square and the other four at the sides of the square perfectly match with positions of the Ag octahedron Ag_6 shown in Figure 1 (left upper corner). The intensity profiles plotted over three atomic columns in the sodalite cages (Figure 4e) show a higher intensity at the corners because of the higher number of atoms in those positions. For the second line intensity profile (points 4, 5, and 6), atoms forming the Ag_6 cluster, the highest value was obtained in the center of the octahedron, again attributed to the greater number of atoms in that column. For those atoms the interatomic distance was found to be 2.70 Å. To confirm all these assignments simulated STEM-HAADF was performed using the model proposed in Figure 4d. The same contrast was obtained for the simulated data and made it possible to unambiguously determine the silver atomic positions. In addition, a faint signal emanating from the Al, Si, O framework can be observed (Figure 4f).

The Ag_6 octahedron did not appear in certain regions of the crystals (Figure 4a), which instead contained clusters in the alpha cages that were absent from the Rietveld refinement (see the Supporting Information S1). This observation suggests that these regions result from the short exposure to atmosphere during the manipulation of the material and preparation of the microgrid. It is likely that water coordinates to the Ag^+ ions in the 6-rings that anchor the neutral Ag_6 clusters in the sodalite cages, drawing them into the alpha cages and releasing the Ag atoms to diffuse through the zeolitic structure, and end up forming larger nanoparticles in the alpha cages or on the surface of the crystals. Thus, the structural conformation of the material under working conditions (i.e. humidity or open atmosphere) differs from the as-synthesized material.

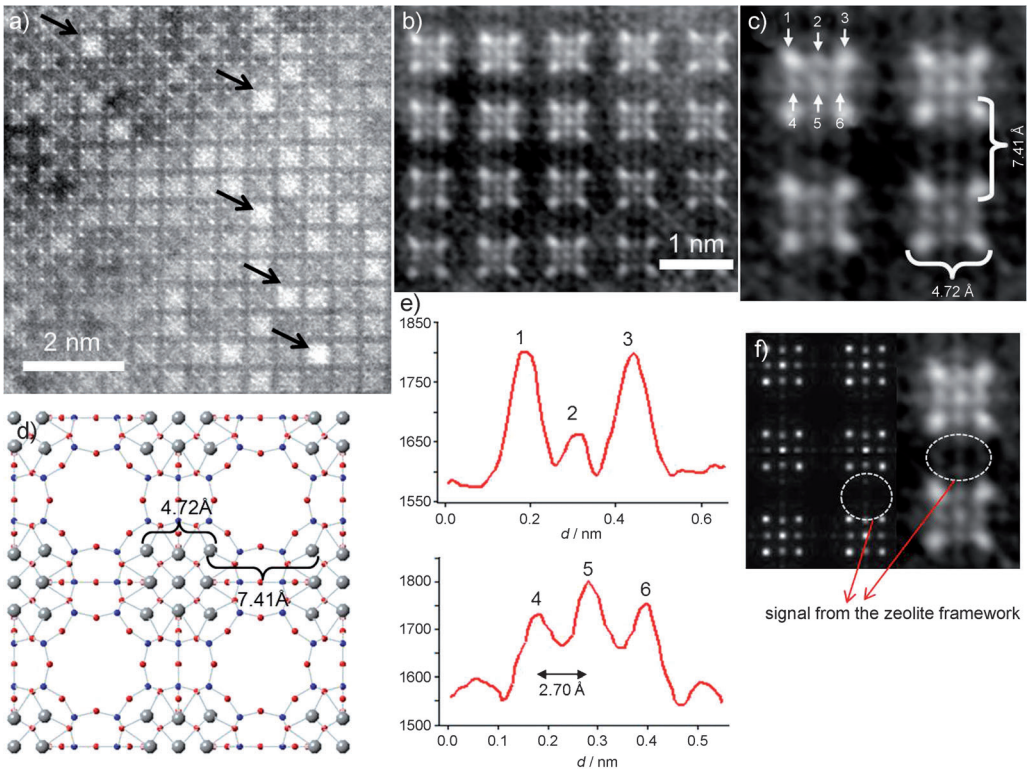

Figure 4. a) Aberration-corrected STEM-HAADF image of the silver zeolite A (AgA) along the [001] direction, where the white spots are single atomic columns and the black arrows point to Ag clusters in the alpha cages. b,c) Fourier-filtered images of the atomic distribution where the four columns of Ag at the corners of the sodalite cage are separated by 4.72 Å and each sodalite cage is separated by 7.41 Å; the Ag_6 cluster is also observed in these cages. d) Proposed model with the Ag atoms in grey. e) Intensity profiles performed on the atoms marked as 1, 2, and 3 in (c) and 4, 5, and 6 with the interatomic distance between these atoms being 2.70 Å. f) Multislice STEM simulation along the [001] direction using 300 kV, $C_s = 0$ mm, a defocus value of 0, a probe convergence semiangle of 24 mrad, and a collection angle of 70–200 mrad. The experimental image is shown alongside, and in both cases the zeolite framework signal is marked by white circles.

In summary, the present results demonstrate the ability of aberration-corrected STEM-HAADF to characterize at atomic resolution zeolite frameworks with different metal cations incorporated in the structure. The fact that the Si/Al ratio was 1:1 represents a huge step forward in the applica-

tion of this technique, as it proves its genuine applicability to any of the 176 zeolitic framework types. With these results we have been able to image for the first time the silver arrangement in dehydrated silver-exchanged zeolite A, which was first described by Kim and Seff[15a] in 1977. We have been able to evidence the formation of a silver octahedron inside the sodalite cages surrounded by eight cations, each located in the center of a 6-ring. We observe that these octahedra are less stable in atmosphere which suggests differences between the material as-synthesized and under potential catalytic conditions. This method offers a real solution for in-depth characterization at the atomic level, including pore contents, of three-dimensional porous solids widely employed in the petrochemicals industry, which is essential for a full understanding and better design of new catalysts.

Experimental Section

Synthesis: The sodium zeolite A (NaA) was prepared using a verified standard synthesis for zeolite A.[17] The zeolite (8 g) was then stirred in a solution of $AgNO_3$ (0.1M, Sigma Aldrich, 99%) at room temperature for 16 h. The milky solution obtained was filtered and washed with deionized water (1 L) to remove any salt remaining on the surface. Once the silver ion exchange was completed, the silver zeolite A was dehydrated at 425 °C for 12 h under 1×10^{-6} mbar. The material was then kept under argon in a glovebox before electron microscopic examination. For these measurements the vial was opened to air and deeply crushed using a mortar and pestle to obtain the thinnest crystals possible. Afterwards, the zeolite was dispersed in ethanol and a few drops of the suspension were deposited onto the lacey carbon copper microgrids (the total time of the procedure did not exceed 5 min).

Characterization: Powder synchrotron X-ray diffraction profiles were collected on beamline I11 ($\lambda = 0.825035$ Å) at the Diamond Light Source, UK. All samples were loaded into borosilicate glass capillaries of 0.5 mm diameter and sealed using a small blowtorch flame. The scattered radiation was detected as a function of 2θ (scattering angle) by the multi-analyzing crystals (MAC) detector with a step size of 0.005°.

Aberration-corrected STEM-HAADF data was acquired using a XFEG FEI TITAN 60–300 kV located at the Laboratorio de Microscopias Avanzadas LMA in the Institute of Nanoscience of Aragon (INA). This microscope was equipped with a high-brightness field emission gun (XFEG), a monochromator, and a CEOS dodecapole aberration corrector for the electron probe. A beam convergence of 24.8 mrad half-angle has been used, yielding a calculated probe size of 0.7 Å. Figure 4b,c was Fourier-filtered with the purpose of improving the signal-to-noise ratio (raw data is presented in the Supporting Information S5).

Multislice STEM simulations: To simulate the STEM-HAADF data of the NaA and AgA zeolites along the [001] orientation we used the QSTEM program.[18] The dynamic scattering simulation is based on the multislice method. The crystal supercell dimensions used were $98.64 \times 98.64 \times 981.7$ Å^3, where a maximum thickness of 981.7 Å^3 has been found to be the limit which gives the best fit to the experimental results. The parameters used were: $C_s = 0$ mm, $U_{acc} = 300$ kV, a HAADF collection angle of 70 to 200 mrad, and a convergence semiangle of 24 mrad. For NaA the beam diameter was set to 1.7 Å; for AgA it was set to 0.7 Å.

Received: August 2, 2011
Published online: September 28, 2011

Keywords: catalysts · electron microscopy · mesoporous materials · nanomaterials · zeolites

[1] C. Baerlocher, L. B. McCusker, http://www.iza-structure.org/databases/books/Atlas_6ed.pdf, **2011**.
[2] A. Corma, *Chem. Rev.* **1997**, *97*, 2373–2419.
[3] A. Philippou, M. W. Anderson, *J. Am. Chem. Soc.* **1994**, *116*, 5774–5783.
[4] T. Masuda, T. Asanuma, M. Shouji, S. R. Mukai, M. Kawase, K. Hashimoto, *Chem. Eng. Sci.* **2003**, *58*, 649.
[5] a) L. A. Bursill, E. A. Lodge, J. M. Thomas, *Nature* **1980**, *286*, 111–113; b) O. Terasaki, T. Ohsuna, V. Alfredson, J.-O. Bovin, D. Watanabe, K. Tsuno, *Ultramicroscopy* **1991**, *39*, 238–246; c) O. Terasaki, T. Ohsuna, *Top. Catal.* **2003**, *24*, 13–18; d) J. Meurig Thomas, P. A. Midgley, *Chem. Commun.* **2004**, *1253–1267*, 1253–1267; e) I. Díaz, E. Kokkoli, O. Terasaki, M. Tsapatsis, *Chem. Mater.* **2004**, *16*, 5226–5232; f) M. Choi, K. Na, J. Kim, Y. Sakamoto, O. Terasaki, R. Ryoo, *Nature* **2009**, *461*, 246–250; g) I. Díaz, A. Mayoral, *Micron* **2011**, *42*, 512–527; h) J. E. Readman, P. D. Barker, I. Gameson, J. A. Hriljac, W. Zhou, P. P. Edwards, P. A. Anderson, *Chem. Commun.* **2004**, 736.
[6] a) M. M. J. Treacy, J. M. Newsam, *Ultramicroscopy* **1987**, *23*, 411–420; b) R. Csencsits, R. Gronsky, *Ultramicroscopy* **1987**, 421.
[7] L. A. Bursill, J. M. Thomas, K. J. Rao, *Nature* **1981**, *289*, 157–158.
[8] R. F. Egerton, P. Li, M. Malac, *Micron* **2004**, *35*, 399–409.
[9] V. Ortalan, A. Uzun, B. C. Gates, N. D. Browning, *Nat. Nanotechnol.* **2010**, *5*, 506–510.
[10] a) O. L. Krivanek, N. Delby, A. R. Lupini, *Ultramicroscopy* **1999**, *78*, 1; b) P. E. Baston, N. Dellby, O. L. Krivanek, *Nature* **2002**, *418*, 617.
[11] A. Mayoral, D. A. Blom, M. M. Mariscal, C. Guiterrez-Wing, J. Aspiazu, M. Jose-Yacaman, *Chem. Commun.* **2010**, *46*, 8758–8760.
[12] a) Y. Inouea, M. Hoshino, H. Takahashi, T. Noguchi, T. Murata, Y. Kanzaki, H. Hamashima, M. Sasatsu, *J. Inorg. Biochem.* **2002**, *92*, 37–42; b) Y. Matsumura, K. Yoshikata, S. Kunisaki, T. Tsuchido, *Appl. Environ. Microbiol.* **2003**, *69*, 4278–4281.
[13] a) T. R. Thomas, B. A. Staples, L. P. Murphy, *Vol. 4088737*, United States, **1978**; b) O. B. Yang, Y. J. Kim, J. C. Kim, J. S. Lee., H. J. Yang, *Vol. 5457230*, United States, **1995**.
[14] P. A. Anderson, *Molecular Sieves*, *Vol. 3*, Springer, Berlin, **2002**.
[15] a) Y. Kim, K. Seff, *J. Am. Chem. Soc.* **1977**, *99*, 7055–7057; b) A. Mayoral, P. A. Anderson, *Nanotechnology* **2007**, *18*, 165708.
[16] P. A. Jacobs, J. B. Uytterhoeven, H. K. Beyer, *J. Chem. Soc. Faraday Trans.* **1979**, *75*, 56.
[17] H. Robson, K. P. Lillerud, *Syntheses of Zeolitic Materials*, 2nd ed., **2001**.
[18] C. T. Koch, Arizona State University **2002**.

